

Journal Pre-proof

Monitoring intermediate species formation by DRIFT during the simultaneous removal of soot and NO_x over LaAgMnO₃ catalyst

Laura Urán, Jaime Gallego, Wilson Ruiz, Esther Bailón-García, Agustín Bueno-López, Alexander Santamaría



PII: S0926-860X(19)30435-1
DOI: <https://doi.org/10.1016/j.apcata.2019.117280>
Reference: APCATA 117280

To appear in: *Applied Catalysis A, General*

Received Date: 12 August 2019
Revised Date: 13 September 2019
Accepted Date: 1 October 2019

Please cite this article as: Urán L, Gallego J, Ruiz W, Bailón-García E, Bueno-López A, Santamaría A, Monitoring intermediate species formation by DRIFT during the simultaneous removal of soot and NO_x over LaAgMnO₃ catalyst, *Applied Catalysis A, General* (2019), doi: <https://doi.org/10.1016/j.apcata.2019.117280>

This is a PDF file of an article that has undergone enhancements after acceptance, such as the addition of a cover page and metadata, and formatting for readability, but it is not yet the definitive version of record. This version will undergo additional copyediting, typesetting and review before it is published in its final form, but we are providing this version to give early visibility of the article. Please note that, during the production process, errors may be discovered which could affect the content, and all legal disclaimers that apply to the journal pertain.

© 2019 Published by Elsevier.

Monitoring intermediate species formation by DRIFT during the simultaneous removal of soot and NO_x over LaAgMnO₃ catalyst

Laura Urán^a, Jaime Gallego^a, Wilson Ruiz^a, Esther Bailón-García^b, Agustín Bueno-López^b, Alexander Santamaría^{a,*}

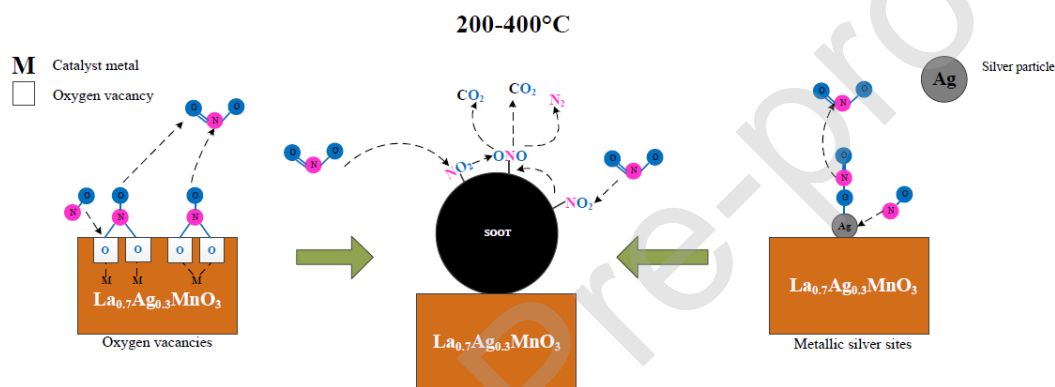
^a Química de Recursos Energéticos y Medio Ambiente, Instituto de Química, Facultad de Ciencias Exactas y Naturales, Universidad de Antioquia (UdeA), Calle 70 N° 52-21, 1226 Medellín, Antioquia, Colombia

^b Departamento de Química Inorgánica, Universidad de Alicante, Carretera de San Vicente s/n. E03080, Alicante, España

*Corresponding author.

E-mail address: alexander.santamaria@udea.edu.co (A. Santamaría)

Graphical abstract



Highlights

- O-vacancies and Ag(s) over La_{0.7}Ag_{0.3}MnO₃ are the most active sites for NO and oxygen adsorption.
- Chelating and bridging nitrates along with Ag-nitrites are the primary reaction intermediates for the NO oxidation.
- Monodentate nitrates and Ag-nitrates were considered NO_x storage species over 400 °C.
- A reaction pathway for soot and NO removal over La_{0.7}Ag_{0.3}MnO₃ was proposed based on DRIFT results.
- The silver-free catalyst was less active than its counterpart due to changes in nitrogenous species distribution.

Abstract

The microwave-synthesized-LaAgMnO₃-catalyst can eliminate soot and NO_x simultaneously below 400 °C. To get some insight about the chemical species formed on catalyst and soot surfaces, in situ

diffuse reflectance infrared Fourier transform (DRIFT) spectroscopy under NO, O₂, and NO/O₂ atmospheres was performed. The DRIFTS results indicated that over 200 °C, at least four types of nitrate-species, mono- and bi-dentate nitrates (bridging and chelating) on the perovskite, as well as Ag-nitrite/nitrate, with different thermos-stabilities were formed. The decomposition of less stable surface nitrates/nitrites accounts for NO₂ formation which assisted soot oxidation. The transformation-decomposition of nitrite/nitrate compounds coincided with the appearance of CO₂ and carbonate-species coming from re-adsorption of soot combustion products. Monodentate nitrates, which are more stable nitrate-species, were considered NO_x storage-species over 400 °C. Chelating- and bi-dentate nitrates formed on perovskite oxygen vacancies appear to be the primary reaction intermediates for the NO oxidation reaction over the Ag-doped perovskite catalyst.

Keywords: Silver containing perovskite, DRIFT, soot-NO_x removal, activation energy, nitrogenous species, NO₂.

1. Introduction

NO_x and soot emissions from mobile diesel engines are one of the major contributors to air pollution causing severe environmental and human health problems [1-3]. Future environmental standard regulations will lead to the integration of depollution systems for these two pollutants in all types of vehicles [3, 4]. Exhaust-after-treatment devices and engine modifications have been implemented to reduce the NO_x and soot emissions from diesel engines [5-9]. However, for the simultaneous removal of soot and NO_x, it is not enough to consider only engine modifications, and the implementation of diesel particle filter combined with catalytic combustion technology appears to be the most practical method to reduce the emission of these harmful substances [9-13].

Generally, NO₂-assisted catalytic combustion of soot (known as continuously regenerating trap-CRT) involves two steps. First, NO is catalytically oxidized to produce NO₂, which is a strong oxidizer that reacts with soot collected on a filter placed downstream at a temperature much lower than that required for either NO and/or O₂ combustion [9-19]. The main reaction products of the soot-NO₂ reaction are NO and CO₂, although few NO_x can be reduced until N₂. In spite of the positive effect of NO_x on soot combustion is well-known in the literature, there are still some issues to be investigated about the reaction mechanism for certain catalysts [17, 18, 20].

In the pioneer work of Shangguan et al. [19], they proposed a mechanism for the simultaneous removal of soot and NO_x involving several steps that are temperature dependent. They suggested that the NO₂ formed in the gas phase is adsorbed dissociatively on the catalyst surface as NO_{ad} and

O_{ad} . Then, the NO_{ad} reacts with an active carbon site leading to the formation of $C^*[N,O]$ complexes on soot particle surface. These complexes react with another NO_{ad} species adsorbed on catalyst releasing CO_2 to the gas phase and increasing the population of N-containing intermediates on soot surface. In a further reaction step, these intermediates can be released as molecular nitrogen (N_2). However, they did not give additional information about the type of complexes formed on the catalyst and soot surfaces.

Later on, it was demonstrated through in-situ diffuse reflectance Fourier transformed (DRIFT) data, that when catalysts were exposed to a $NO + O_2$ mixture, nitrates and nitrites species were formed on metal sites. However, the kind of nitrogenous species will depend on the metallic site on catalyst. For instance, Bin et al [15], evidenced the formation of chelating bridging and monodentate nitrates on MnO_x sites on $La_{0.8}Ce_{0.2}Mn_{0.7}Bi_{0.3}O_3$ catalyst. Zhu et al. [20], confirmed that bridged bidentate nitrites were the main adsorbed species over CeO_2 and transition-doped ceria ($M_{0.1}Ce_{0.9}O_2$) catalysts, since the bridged bidentate nitrates were scarcely observed. Ait et al. [21], also evidenced the formation of chelating nitrites, bidentate and monodentate nitrates on $La_2Sn_{2-y}Co_y$ catalyst. Bin et al. [15], on the other hand, presented information not only of the type of nitrates formed in the catalyst surfaces but also on the soot particle surfaces, as evidence of the interaction of the three components of the system (soot/ O_2 / NO_x).

Currently, perovskite-like materials, with ABO_3 general formula, are probably one of the most studied mixed-oxide system in the field of heterogeneous catalysts due to their versatility to adopt a wide range of different compositions, changing either the A or the B cation or partially substituting each cation by other cations of the same or different valences. D.Y. Yoon et al. [22], have found that the partial substitution of La^{3+} with Ag^+ in $LaMnO_3$ perovskite catalyst produced oxygen vacancies as active reaction sites for the NO oxidation reaction involving the formation of both mono- and bi-dentate nitrate species as the major reaction intermediates during the oxidation of NO to NO_2 . However, this reaction was performed without soot and in a very low temperature range. In the present work, we address the NO-assisted soot combustion process over $LaAgMnO_3$ catalyst to obtain further information about the main intermediates complexes formed on both catalyst and soot surfaces. This catalyst has demonstrated to be very active for the simultaneous removal of soot and NO and the presence of silver into the structure improved the catalytic performance of the solid [22, 23].

2. Experimental

2.1 Sample preparation

LaMnO₃ and La_{0.7}Ag_{0.3}MnO_{δ±3} (referred to as LaAgMnO₃) perovskite-like catalysts were synthesized by the microwave-assisted (MW) methodology according to our previous paper [23], since it has been proven that this methodology can improve the incorporation of silver into the perovskite structure [23]. Metal nitrate precursors (La(NO₃)₃·6H₂O (Merck), AgNO₃ (Merck), and Mn(NO₃)₂·4H₂O (Merck)) to prepare 1 gr of catalyst were dissolved in 20 mL of deionized water, and exposed to ultrasound irradiation for 30 min; with a subsequent stirring for 6 h. Then, the resulting solution was subjected to microwave irradiation in a simple domestic oven (AS-HM-1.1 ME GRILL INOX, at 2.45 GHz) with an output power of 700 W for 6 min. Finally, the obtained solid was calcined in air at 600 °C for 1 h.

2.2 Catalyst characterization

To study catalysts structure X-ray diffraction and Raman spectroscopy analysis were used. XRD experiments were performed on a X-ray Panalytical X'PERT PRO MPD diffractometer, using Cu K_α radiation ($\lambda = 1.5406 \text{ \AA}$) at 45 kV and 40 mA; the 2θ angle in the range 10°-70°, with step size 0.013° and step time of 59.31 s. Raman spectra were obtained using a LabRam HR Horiba microscope system equipped with a 632.8 nm He/Ne laser excitation source. For each catalyst sample, four different spots were analyzed in a spectral range of 800 cm⁻¹ -2000 cm⁻¹ using a magnification objective of 50x. A laser power of 1.7 mW (10% of the total power); grating of 600 lines/mm; exposure time of 1 s; acquisition time of 10 s and an average of 10 scans were used as reference conditions to obtain good readings in the spectra. Catalyst Morphology was observed by SEM (JEOL 7100F Field Emission Gun-Scanning Electron Microscope (FEG-SEM) at 15 kV); and TEM (Tecnai F20 Super Twin TMP), at an accelerating voltage of 200kV. X-ray photoelectron spectroscopy (XPS) was used to characterize the surface composition. XPS analysis were carried out in a Thermo Fisher Scientific equipment, using a voltage of 20 kV, a current of 20 mA, and Al K_α as radiation source. The binding energies were calibrated by setting C1s transition at 284.6 eV, as an internal standard.

2.3 Catalytic performance

Soot oxidation activity and NO_x elimination performance of the prepared catalysis were tested using temperature-programmed oxidation test. A detailed description of the equipment and the experimental procedure has been previously reported in a previous paper of ours [23]. All the

experiments were carried out in tight contact conditions, mixing 5 mg of soot (carbon black, FW200, from Orion Engineering) with 45 mg of catalyst (1:9 weight ratio) in an agate mortar for 10 min. The soot-catalyst mixture was also diluted with 150 mg of quartz sand (SiO_2). The flow at inlet of the reactor, with a rate of 100 mL/min, had a composition of 2000 ppm NO/ 10% vol. O_2 / He. Gas composition at reactor outlet was determined by mass spectrometry, following signal intensities $m/z = 12, 14, 16, 28, 30, 44, \text{ and } 46$; and an electrochemical analyzer (KIGAZ 310) to measure the NO and CO concentration. The catalytic activity of the evaluated solids was determined by establishing the temperature for the maximum CO_2 production in the CO_2 evolution curve (named T_{peak}); and the temperature for the 50% of soot conversion (T_{50}). Soot conversion and the selectivity to CO_2 formation (S_{CO_2}) were defined according to reference [23].

2.4 DRIFT experiments

The in situ diffuse reflectance Fourier Transform (DRIFT) spectra were recorded on a Nicolet 6700 apparatus equipped with a Mercury–Cadmium–Telluride (MCT) detector and a Thermo's heating chamber. For the DRIFTS experiments, the soot–catalyst mixture (1:9 weight ratio) in tight contact was then mixed with KBr at a ratio of 1:10 by weight. The powdered mixture was placed into the heating chamber, and then were purged and pretreated with Ar stream (50 mL/min) at 600 °C for 20 min and were then cooled down to 25 °C to remove the surface-adsorbed (H_2O and CO_2) contaminants from the catalyst. During the cooling process, the treated catalyst was taken as background at 50, 100, 200, 300, 350, 400, 450, 500 and 600 °C, respectively. The DRIFT spectra for the in situ combustion experiments were carried out by feeding 2000 ppm of NO/10% O_2 / Ar at a flow rate of 50 mL/min and a heating rate of 5 °C/min. All spectra were recorded by 32 scans accumulation with a resolution of 4 cm^{-1} in the wavenumber range from 1000 cm^{-1} to 4000 cm^{-1} . Similarly, several blank experiments with and without soot under different atmospheres (Cat-NO, Cat- O_2 , Cat- O_2 /NO, Cat-Soot- O_2 , Cat-soot- O_2 /NO, etc) were carried out to complete the analysis.

3. Results

3.1 Catalyst characterization

Fig. 1 shows the X-ray diffraction patterns for LaAgMnO_3 and LaMnO_3 catalysts obtained under similar conditions. The large peak observed at 32 ° confirmed the perovskite crystalline phase formation which agrees well with the reported data (ICDD 32-0484). These results suggest that the

addition of silver did not modify the parent structure, due to the similarity of the ionic radius between La^{3+} (1.36 Å) and Ag^+ (1.28 Å). The sharp and strong diffraction peaks indicate that these samples were well crystallized and the average crystalline domain calculated by using the Debye Scherrer formula was around 15-25 nm for both cases. These values agree with those reported in [23] which was calculated by HRTEM. For the containing silver catalyst (LaAgMnO_3), the signals appearing at 2θ values of 38.3° , 44.5° and 64.6° , corresponding to metallic silver (Ag^0), indicate that not all silver was incorporated into the perovskite lattice. Besides the metallic silver segregation observed in LaAgMnO_3 , the XRD pattern of these perovskites sample did not show the presence of secondary phases associated to La_2O_3 (ICDD 2-0688), MnO_2 (ICDD 4-0378) and Ag_2O (ICDD 12-0793) oxides as segregated phases. A previous study suggests that the way this material can be synthesized may play an important role in the perovskite catalyst activation, finding that microwave-assisted synthesis improves the incorporation of Ag into the perovskite lattice structure increasing the number of oxygen vacancies and the availability of metallic silver onto the surface, both active for the assisted oxidation of soot by NO_x [23].

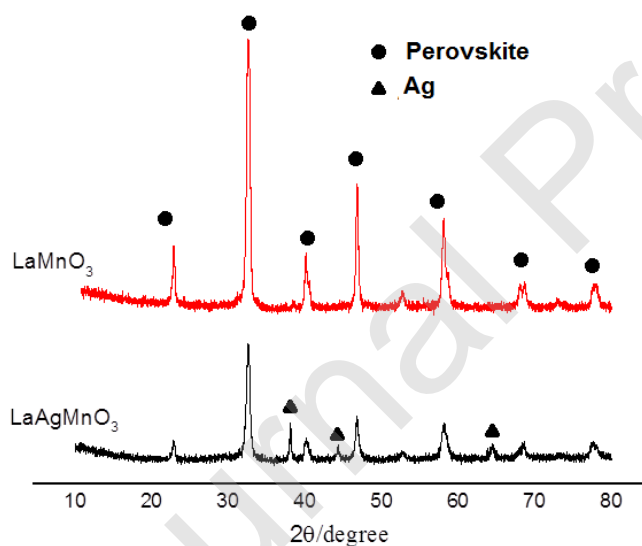


Fig. 1. X-ray diffractogram of LaAgMnO_3 and LaMnO_3 catalysts.

Raman scattering measurements of both LaMnO_3 and LaAgMnO_3 presented in Fig. 2 also confirmed the formation of the perovskite-like phases. This Raman feature is typical of manganites, and it is almost independent of the crystallographic symmetry (orthorhombic or rhombohedral) [25]. In Fig. 2, two high frequency modes, Ag ($\sim 496 \text{ cm}^{-1}$) and B1g ($\sim 620 \text{ cm}^{-1}$), corresponding to anti-symmetric and symmetric in-plane vibrations associated to Jahn Teller (JT) distortions of the corner-shared oxygen octahedra in LaMnO_3 were observed. However, it was noted that the

intensities ratio associated with JT distortion (I_{A_g}/I_{B_g}) decreases in the Ag-doped catalyst. In fact, the decrease in the JT distortions observed in the LaAgMnO_3 catalyst can be associated to an increase in both Mn^{4+} cations formation (or a decrease in Mn^{3+} cations) and oxygen vacancies formation through a charge compensation mechanism caused by the presence of a cation of lower valence, as Ag^+ in the A site cation position [25]. Literature has suggested that the doping process increases the relative volume of distorted areas due to the occurrence of sublattice oxygen disorder broadening some of the first-order Raman lines, but in our case this was just a little perhaps due to the small differences between cation radius as it was pointed out by XRD [25].

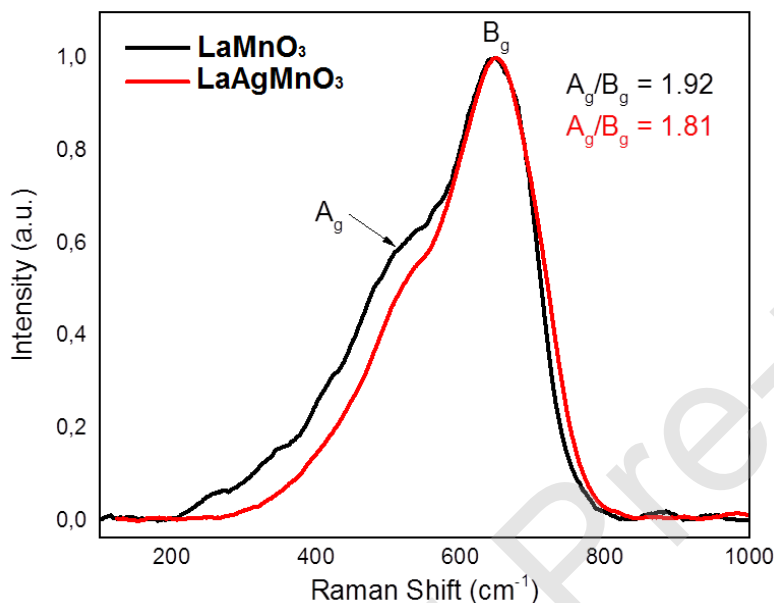


Fig. 2. Raman spectra of LaMnO_3 and LaAgMnO_3

Fig. 3 presents SEM and TEM images of the synthesized samples. SEM images did not show significant difference on particle morphology between the catalysts which present irregular aggregates of soft bumps. The similarity between morphologies was because both solids were exposed to the same synthesis procedure: microwave time (6 min) and power (700 W), along with the same calcination time and temperature. By contrary, TEM images allow to see segregated nanoparticles for LaAgMnO_3 sample (see Fig. 3 B), that according to EDX analysis, it corresponds to metallic silver particles being in good agreement with XPS results.

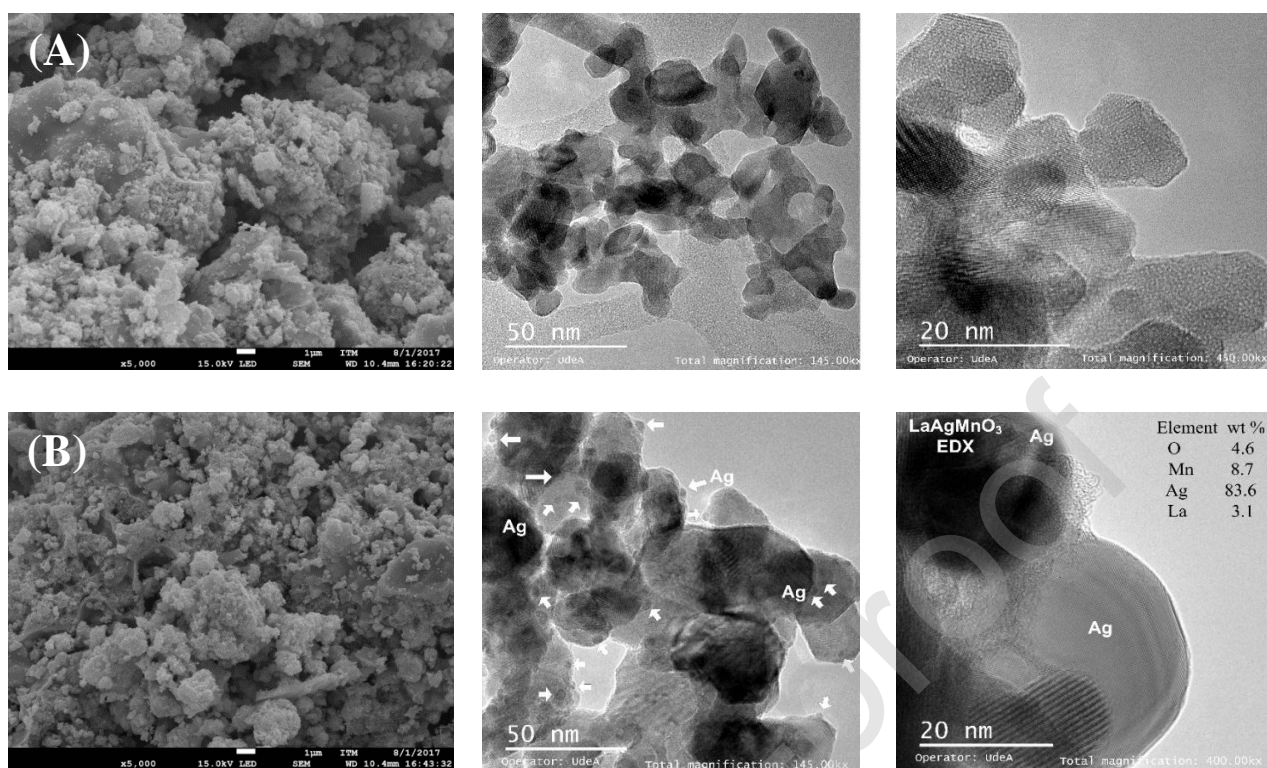


Fig. 3. SEM and TEM images of (A) LaMnO₃ and (B) LaAgMnO₃ with silver particle segregation.

Surface elemental composition and binding energies of La 3d_{5/2}, Ag 3d_{5/2}, Mn 2p_{3/2} and O 1s core levels were measured by XPS for LaMnO₃ and LaAgMnO₃ perovskites. Fig. 4 presents XPS spectra of in the (A) O1s core level (B) Mn2p_{3/2} core level of perovskite-like catalysts.

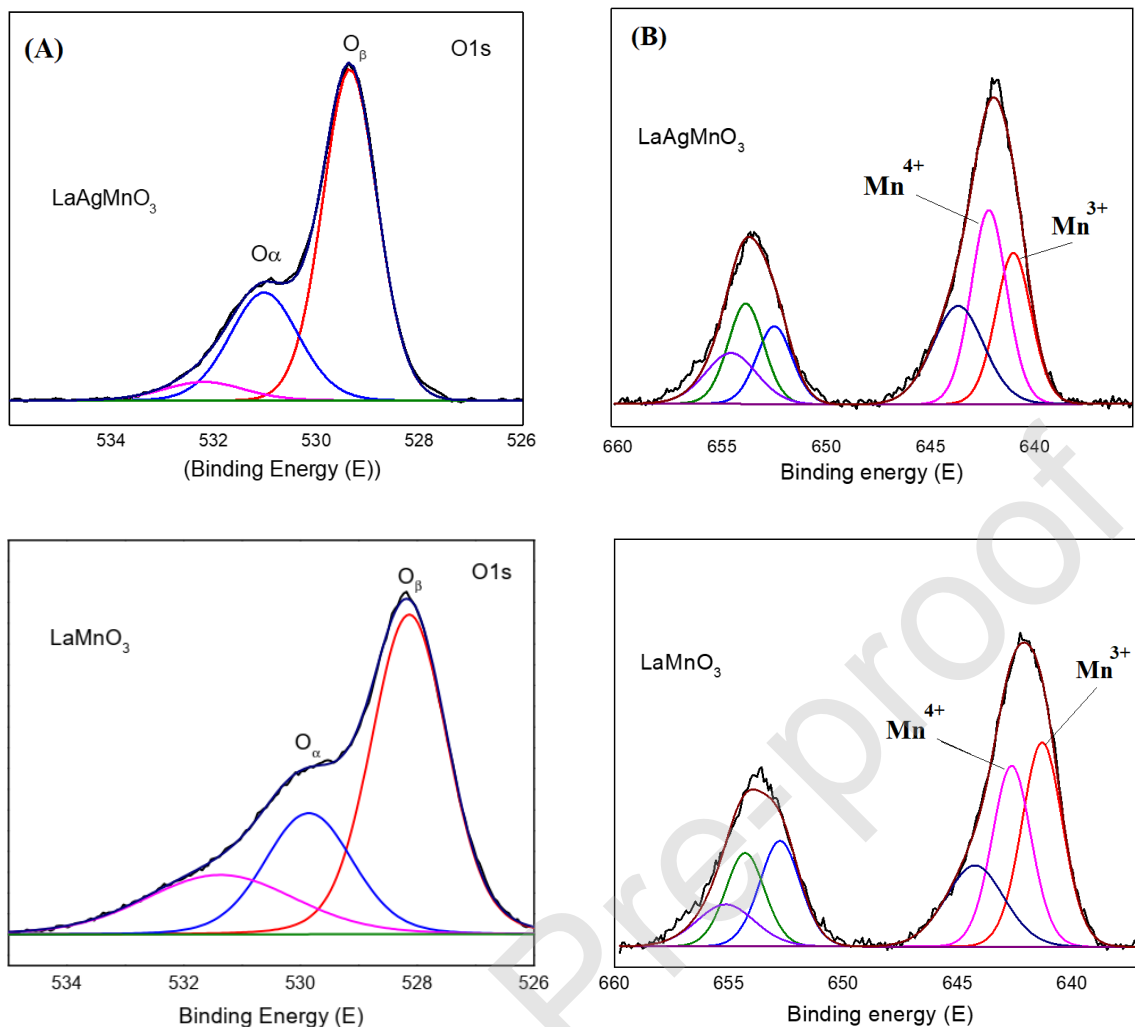


Fig. 4. Decomposed XPS spectra in the (A) O1s core level (B) Mn2p_{3/2} core level of perovskite-like catalysts.

The O1s transition were decomposed into three peaks: the lower binding energy signal, between 528.6 eV and 529.3 eV, was attributed to lattice oxygen (O_β); intermediate binding energy peak at 531 eV corresponds to adsorbed oxygen (O_α), associated with surface vacancies (O⁻ or O²⁻ species); the highest binding energy, around 533.0 eV, it has been attributed to superficial water and hydroxyl groups [23, 26, 27]. The Mn2p_{3/2} binding energy spectra was deconvoluted in three signals, in Fig. 4B, corresponding to Mn³⁺ (641.3 eV), Mn⁴⁺ (642.3 eV), and a weak satellite (644.0 eV) of the Mn2p_{3/2} [28, 29]. The Ag3d_{5/2} spectra, shown in the supplemental material (**Fig.S1**), presents three contributions associated to metallic silver (Ag⁰) at 368.2 eV, segregated silver oxide (Ag₂O) at 367.7 eV and silver incorporated into perovskite structure (Ag⁺) at 367.3 eV [30]. In Table 1, It is possible to see that the Ag-doped perovskite presented an Ag/Mn atomic ratio higher than the stoichiometric one, indicating that part of the silver was segregated on catalyst surface

mainly as silver oxide (Ag_2O) and metallic silver (Ag°). In fact, 30% of the non-incorporated silver (Ag) corresponds to the metallic silver (Ag°).

As was stated before, the charge compensation mechanism in perovskite-like catalyst can be either by oxygen vacancies formation and/or by the shifting of B cation toward higher valences (e.g., Mn^{3+} to Mn^{4+}) [25]. Therefore, the increase in the $\text{Mn}^{4+}/\text{Mn}^{3+}$ atomic ratio, as well as, the increase in the surface oxygen content, (O_a), reported in Table 1 suggests that both processes contribute to the charge compensation mechanism when silver incorporation into the LaMnO_3 catalyst was achieved being in good agreement with the Raman results. On the other hand, contrary to what was observed in XRD, the results of XPS confirmed the segregation of lanthanum as La_2O_3 on the catalyst surface (the La $3d_{5/2}$ spectrum can be found in **Fig. S2**). The difference in the response between the two analytical techniques could be associated to difference in the sampling depth.

3.2 Catalytic test for the simultaneous removal of Soot and NO_x

Fig. 5 A) illustrates the species evolution profile (CO_2 , NO , N_2) as a function of temperature during the simultaneous soot and NO_x removal over LaAgMnO_3 catalyst synthesized by microwave.

While, Fig. 5 B) shows the soot conversion profiles of different blank experiments performed with and without NO over LaAgMnO_3 . Also, for comparison purposes, the species evolution profiles of non-catalytic system and the one over LaMnO_3 without silver were introduced. In Fig. 5A, the dash dotted line represents the NO concentration in the gas inlet and the points below and above this line imply the occurrence of NO adsorption/desorption or reduction, respectively.

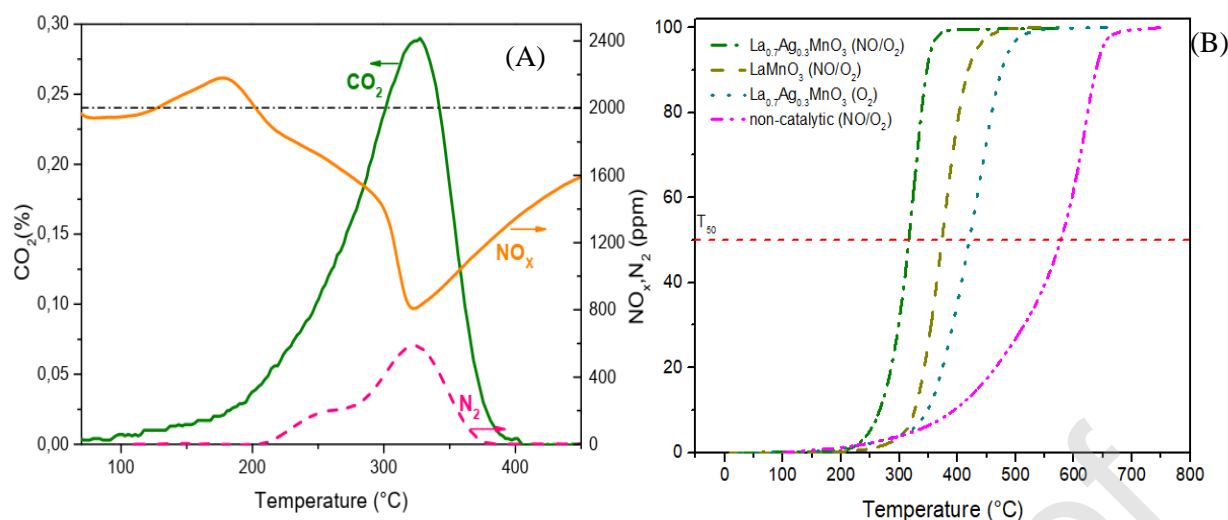


Fig. 5. (A) CO₂, N₂, and NO species evolution during simultaneous removal of soot and NO over La_{0.7}Ag_{0.3}MnO₃ and (B) soot conversion to CO₂ coming from different experiments.

At temperatures below 200 °C, two consecutive events associated to the adsorption/desorption process of weakly NO molecules bounded to catalyst surface were seen. It is interesting to note that the NO desorption peak coincides with the soot ignition temperature of around 124 °C, then decrease completely up to 200 °C where the beginning of the N₂ evolution or NO reduction process is marked. This reduction process continues as long as there is soot in the reaction medium, which in this case is up to 400 °C. However, it is noteworthy that during this temperature range the slopes in the NO reduction profile change, indicating that at least two types of nitrogen species linked to some catalyst surface sites are evolving as N₂ when soot oxidation is taking place. One of these sites produces a local maximum in N₂ evolution of around 260 °C, while the other one produces a global maximum in N₂ evolution near to 320 °C. This global maximum coincides perfectly with both the maximum NO consumption and the maximum CO₂ evolution. This result is a clear evidence of the simultaneity of soot and NO removal process. On the other hand, after 400 °C the evolution of NO continues to increase gradually until 600 °C without reaching the reference NO concentration of 2000 ppm. However, this process is not associated with a reduction event since the evolution of N₂ ended just when the soot combustion was completed. Therefore, the behavior observed in the NO profile after 400 °C can be explained through the formation of thermally stable NO_x complexes on storage active sites on catalyst surface which would also explain why the NO curve did not reach the reference concentration at 600 °C. On the other hand, in the silver-free perovskite (LaMnO₃), the NO_x storage capacity was reduced since no further adsorption was observed above 400 °C as occurred over LaAgMnO₃, See **Fig. S3** of the supporting material. This behavior can be explained by considering that silver catalyzed the NO to NO₂ oxidation process (as evidenced in soot-free

catalytic test to follow the NO oxidation, presented in **Fig. S4**), being NO₂ a specie that chemisorbs better than NO, resulting in the promotion of the storage process.

Fig. 5B shows the soot conversion profiles as a function of temperature for the LaAgMnO₃ catalyst under O₂ and NO/O₂ atmospheres, respectively. For comparison purposes the non-catalytic combustion profile as well as the LaMnO₃-catalysed reaction was also taken into account. In general, it can be seen that all catalytic systems showed very good performance in soot oxidation compared to the non-catalytic one according to the following order in activity LaAgMnO₃ (NO/O₂) > LaMnO₃ (NO/O₂) > LaAgMnO₃ (O₂) > non-catalytic (NO/O₂). Similar trends were obtained by Dhal et al [13], who evaluated the effect of Ag and K substitutions on LaMnO₃ catalyst in the simultaneous removal of NO_x and soot. They have found that soot combustion, as well as, the NO_x reduction by soot greatly increase by the presence of metallic silver in the catalyst. In fact, when the partial substitution of Ag into the parent perovskite was around 30% the activity toward the simultaneous removal of NO_x and soot was maximized. They also stated that the dual substitution of silver and potassium promotes simultaneous removal than the catalyst that only contains silver, particularly when the substitution amount of K was around 25%.

Also note that the catalytic oxidation of soot using the Ag-doped perovskite catalyst under NO/O₂ atmosphere showed the lowest activation energy among the evaluated systems (55 kJ / mol) and presented the narrowest oxidation window with a maximum temperature around 327 °C. This value is close to the ones reported by other authors using similar catalytic systems under NO+O₂ and NO₂ atmospheres [19,31,32]. In addition, the NO conversion was near 60%, with a selectivity of 20% towards N₂ calculated on the NO input concentration basis. At this point, it is worth to highlight the importance of silver species, (Ag⁰, Ag⁺, Ag₂O), in the catalytic activity achievement for the removal of both pollutants, particularly when comparing the activity of LaMnO₃ and LaAgMnO₃ catalysts. According to our previous work [23], it was observed that catalyst with higher silver incorporation into perovskite structure (Ag⁺) presented more oxygen vacancies (higher O_v/O_{tot} ratio) and therefore higher catalytic activity. Regarding metallic silver (Ag⁰) segregated on the catalytic surface, it was found that this active site can promote the spill-over phenomena facilitating not only the oxygen and NO activation but also their transfer to soot particles, especially during NO_x-assisted soot oxidation process [23]. Conversely, Ag₂O does not significantly contribute to soot and/or NO_x elimination, since the catalyst with the highest Ag₂O segregation in reference [23] did not imply an enhancement in the catalytic activity due to a decrease in the active surface area.

On the other hand, the positive effect of the presence of NO was also confirmed when comparing the catalytic performance of LaAgMnO₃ catalysts under O₂ and NO/O₂ atmospheres, respectively.

In both cases, the presence of silver and NO into the catalytic systems leads to the formation of active intermediary species that are much more reactive than molecular oxygen thus accelerating the soot oxidation reaction.

3.3 DRIFT analysis results

The nature of the nitrogenated and oxygenated species on the surface of catalyst and soot during the temperature programmed experiments were monitored by DRIFT spectroscopy. However, before showing the experiments of simultaneous soot and NO_x removal, some blank experiments were carried out in order to obtain more information about the kind of intermediate species that are formed during reaction. Table 3 compiles the main chemical species formed on soot surface and catalyst surface when the LaAgMnO₃ catalytic system was exposed to O₂, NO and NO/O₂ respectively. Then, it is shown the infrared spectra of the same catalytic system acting in soot oxidation under O₂ and NO/O₂ atmospheres. And finally, to evaluate the effect of silver incorporation into the perovskite structure on the different chemical species formed during soot oxidation under NO/O₂ environment, the infrared spectra over a reference catalyst (LaMnO₃) were also included.

All experiments were carried out between room temperature and 600 °C at a total gas flow rate of 50 mL/min. Prior to adsorption experiments, the catalysts were treated at 600 °C in Ar for 20 min to remove adsorbed species (e.g., H₂O and CO₂). Then, the samples were cooled down to ambient temperature and the required gaseous atmosphere for reaction was introduced into the sample cell. All spectra were analyzed within the wavenumber region of 4000-1000 cm⁻¹ where the most relevant bands due to nitrogen- and carbon-containing species appear. Table 3 summarizes the main infrared signals due to nitrogen- and carbon-containing species that may be present on catalyst and/or soot samples when they are exposed NO/O₂ environments [16,19,20, 33-66].

3.4 LaAgMnO₃ catalyst exposed to O₂

For LaAgMnO₃ catalyst under O₂ atmosphere (Fig. 6), several signals can be observed, the broad and intense band around 3490 cm⁻¹ is attributed to symmetric and antisymmetric -OH stretching

vibration mode of water adsorbed on catalyst surface, which quickly disappears once the heating process starts [19,22, 33-39]. This signal can also be correlated with the ones observed at 1620 cm^{-1} and 1430 cm^{-1} normally associated with the -OH bending vibration mode of water over Mn atoms [33,69] which also decreased with temperature. However, it was noticed that after $200\text{ }^{\circ}\text{C}$ these signals remain constant with temperature and only the low intense band at 1587 cm^{-1} attributed to OH groups vibration on $\text{La}(\text{OH})_3$ could survive the thermal process due to its high stability [55, 67,68] Although the formation of $\text{La}(\text{OH})_3$ through the La_2O_3 hydration under atmospheric conditions has been suggested in some studies [55, 68] involving perovskite synthesis, its contribution is pretty low as it was confirmed by XPS.

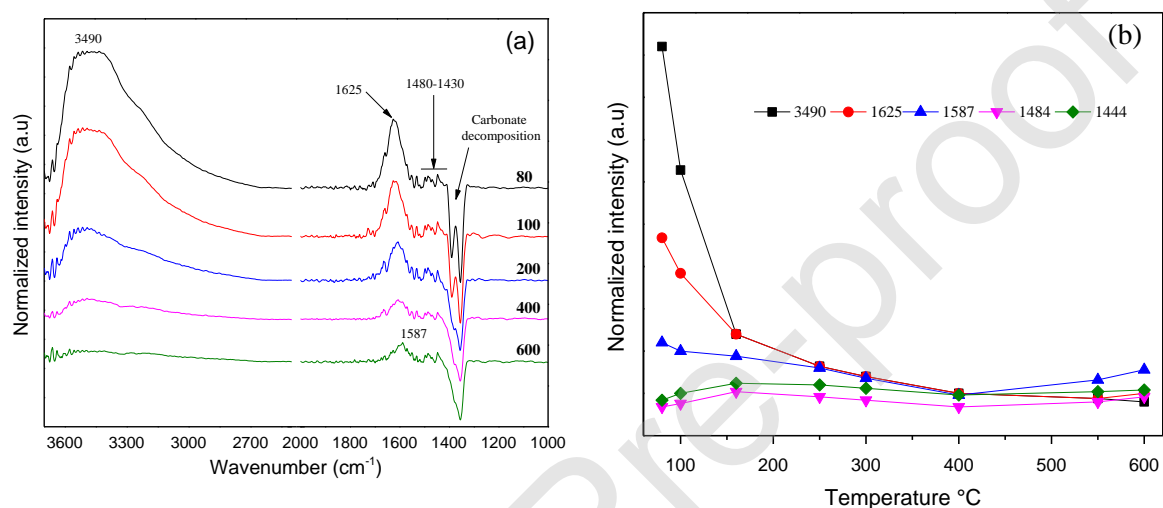


Fig. 6. (A) DRIFT spectra of LaAgMnO_3 catalyst under O_2 atmosphere as a function of temperature and (B) Absorbance intensity variation of different IR signals with temperature.

An interesting feature that was seen in this catalytic system ($\text{LaAgMnO}_3 + \text{O}_2$) was the appearance of a negative peak between 1260 cm^{-1} and 1400 cm^{-1} associated to residual carbonate species decomposition that were previously adsorbed on catalyst surface during synthesis or by catalyst exposition to ambient air where CO_2 can be allocated on oxygen active sites of the type M-O-M [22,43,48] according to this reaction sequence: $\text{M-O-M} + \text{CO}_{2(\text{g})} \rightarrow \text{M-CO}_3\text{-M}$. However, as temperature increases during the cleaning process, the CO_2 is released and the oxygen active site is regenerated under O_2 atmosphere. In fact, after all these groups were removed from the surface, the active sites become available for the catalytic combustion of soot assisted by NO_2 as we are going to discuss latter. Fig. 6B shows the absorbance variation of different IR signals as function of temperature where it can be observed that after water was removed all signals were stable and the surface was completely clean for the subsequent soot oxidation experiments.

3.5 LaAgMnO_3 catalyst exposed to NO

Fig. 7A shows the IR signals of the different chemical species adsorbed on the surface of LaAgMnO₃ catalyst when it was exposed to a NO atmosphere, while Fig. 7B shows the IR absorbance intensity variation as a function of temperature. Besides observing a reduction in the signals intensity associated to water desorption (3490 cm⁻¹ and 1620 cm⁻¹) during thermal treatment, new signals appear in the spectra at 1901 cm⁻¹, 1841 cm⁻¹, 1587 cm⁻¹, 1484 cm⁻¹, 1444 cm⁻¹, 1392 cm⁻¹, and 1355 cm⁻¹. The pair signals at 1901 cm⁻¹ and 1841 cm⁻¹ which increases gradually up to 250 °C and then decreases at 400 °C have been attributed to weakly adsorbed NO or nitrosyl. In fact, it is suggested that the nitrosyl formation can be achieved through the coordination of a NO molecule to a Lewis acid site (Mn) via the nitrogen atom [19,37,40,41].

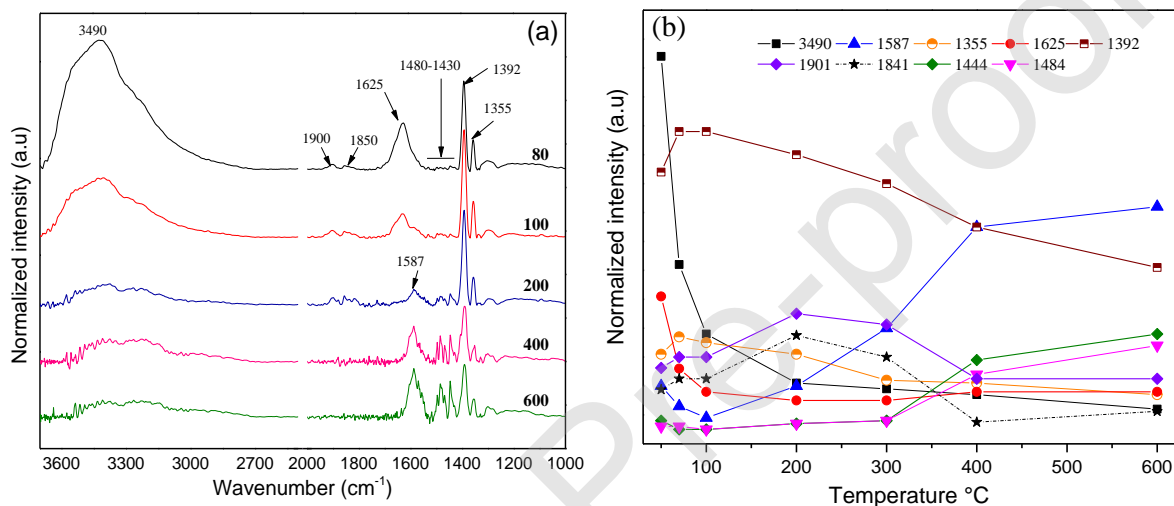


Fig. 7. (A) DRIFT spectra of LaAgMnO₃ catalyst under NO atmosphere as a function of temperature and (B) Absorbance intensity variation of different IR signals with temperature.

The signal at 1587 cm⁻¹ is associated to chelated nitrates that can be obtained through the NO adsorption over two active oxygen sites linked to one metallic species located on catalyst surface [19,22,34,42-45,47-49,51]. Note that this signal gradually increases from 150 °C to 400 °C and then reaches a constant value up to 600 °C. This means that these kinds of nitrates are formed at low temperature mediated by oxygen sites favoring the NO adsorption and, once these sites are saturated, no further NO adsorption can be seen at higher temperature. The nitrate species formation with NO alone can be feasible considering the strong oxidizing properties of manganese-based materials. It has been suggested that the NO⁻ anions exist as transient species in the electron and/or oxygen transfer processes involved in the formation of nitrites according to equation (1) [19,42,48]



Where M-O* is an active oxygen coming from the lattice structure of catalyst through a diffusion mechanism favored by the increase in temperature. Further, the nitrite oxidation can take place by another activated O* surface species according to equation (2). A previous study supports the idea that LaAgMnO₃ catalyst possesses a large quantity of active oxygen not only on the surface (30% is α -O type) but also from the lattice structure of catalyst [23]. Similar behavior was observed for the weak pair of signals at 1444 cm⁻¹ and 1484 cm⁻¹ associated to nitro compounds, as well as, linear nitrites on catalyst surface which rapidly increased from 300 °C to 400 °C where a constant value was reached up to 600 °C giving an idea of their thermal stability, as was previously reported [43]. The notable increment above 300 °C could be associated to the transformation of nitrites species to nitrates species that are stable at higher temperature, since it is known that signals coming from monodentate nitrates or linear nitrates can also be present in this wavenumber range [19,37,42,43,53]. On the other hand, when comparing Fig. 6 and Fig. 7, it is observed that the active sites associated to the negative peak between 1260 cm⁻¹ and 1400 cm⁻¹ were preferentially occupied by NO molecules given place to the formation of two types of nitrogen oxide species at 1390 cm⁻¹ and 1355 cm⁻¹. The signal at 1392 cm⁻¹ has been attributed to the formation of free ionic nitrites species of the type M⁺[NO₂], [34,53] and/or hyponitrites M⁺[ON=NO]²⁻, [25,41,48,54-57], while the signal at 1355 cm⁻¹ is associated to monodentate nitrites [17,22,42-49,52,53,57]. Although these species can be formed at room temperature, their thermal transformation/decomposition under NO atmosphere is much slower than NO/O₂ atmosphere. Some authors have stated that, in the presence of O₂, some nitrites can be easily oxidized and removed as NO₂ at low temperature, which is a key specie for soot oxidation, or turned into stable monodentate nitrates at high temperature. In this regard, even in the absence of O₂ we cannot discard the oxidation of nitrites to monodentate nitrates since it is believed that the active O* species needed for this reaction under NO arise firstly from the own oxygen reservoir in the perovskite catalyst [37,43,53].

3.6 LaAgMnO₃ catalyst exposed to NO/O₂

From Fig. 8, it is possible to see that the presence of O₂ favored the NO adsorption on the LaAgMnO₃ catalyst surface. However, unlike the catalytic tests carried out with NO and O₂ as separated environments, the IR profiles of the catalytic system exposed to an NO/O₂ atmosphere showed some combined features. For example, a low temperature (<200°C) the signals associated to water desorption and the negative peak attributed to carbonate decomposition were seen here and when the catalyst was exposed to O₂.

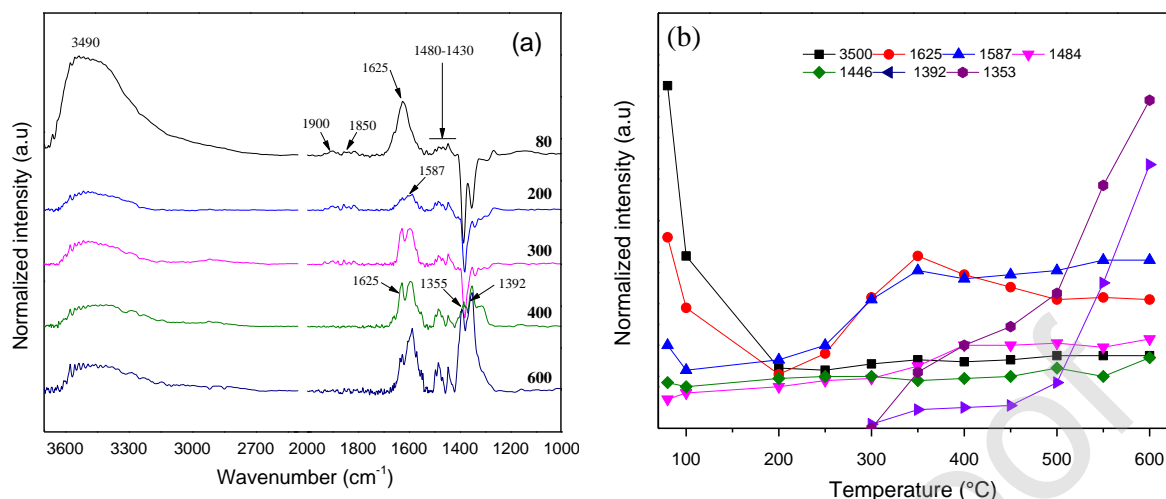


Fig. 8. (A) DRIFT spectra of $\text{La}_{0.7}\text{Ag}_{0.3}\text{MnO}_3$ catalyst under NO/O_2 atmosphere as a function of temperature and (B) Absorbance intensity variation of different IR signals with temperature.

This result suggests that due to the high O_2 relative abundance respect to NO , the competition for the active sites on the catalyst surface is more evident. In this case, the oxygen molecules got adsorbed first blocking the NO adsorption on the active sites of the perovskite. Moreover, as temperature increases above 200 °C, signals associated to nitrates on both the perovskite surface and Ag-sites become significant. Between 200 °C–450 °C it was observed a splitted band with signals at 1620 cm^{-1} and 1587 cm^{-1} corresponding to bridging bidentate nitrates and chelating bidentate nitrates respectively. It is worth to mention that the bridging nitrates signal was only favored in the presence of oxygen since under NO atmosphere was not observed (see Fig. 7). By the time the bridged and chelated nitrates formation is taken place on the catalyst surface, the absolute intensity of the negative peak around 1260 cm^{-1} and 1400 cm^{-1} was reduced until it reaches 300 °C when the peak is reversed and becomes positive. Indeed, the two observed signals at 1380 cm^{-1} and 1355 cm^{-1} emerged from this negative peak suggesting that above 300 °C the ionic nitrates and monodentate nitrates formation under NO/O_2 atmosphere becomes feasible and stable. This supports the idea that molecular oxygen covers large part of the active sites on the catalyst surface accommodating in the vacancies and promoting the oxidation of metallic species, which in turns favors the NO adsorption even at high temperatures. Contrary to what was observed in the catalytic system with NO -only atmosphere, the signals associated to nitrites and/or hyponitrites were not seen in the NO/O_2 case probably due to their easy thermal decomposition in the presence of oxygen [54,56] or due to their replacement by transient nitrates that decompose to NO_2 even at temperatures below 300 °C temperature. Finally, it was observed that above 450 °C, the signal associated to

bridged nitrates decreases in intensity while the signals associated to mono- and bidentate nitrates, as well as free ionic nitrates survived the thermal stress unto 600 °C suggesting not only a good catalytic performance for NO oxidation but also a good NO storage capacity as it was proposed in reference [22,43,49]. The good storage capacity observed in this catalytic system after 400 °C would explain why the NO concentration did not reach the reference value of 2000 ppm at reactor outlet during the soot oxidation experiments assisted by NO (Fig. 5A).

Yoon et al [22], have evidenced the same group of nitrate species including the Ag-nitrates on Ag-doped perovskite ($\text{La}_{1-x}\text{Ag}_x\text{MnO}_3$) catalyst surface during the NO oxidation test. However, they pointed out that as the Ag substitution (x) into the perovskite structure increases from 0.1 to 0.8, the Ag-nitrate peak (1380 cm^{-1}) becomes more evident, while the peak intensities associated to mono- and bidentate nitrates become weaker. This result was attributed in part to the increase of the metallic Ag sites on the catalyst surface, a fact that was not seen in our study since only one Ag composition was evaluated [22]. They also stated that the partial substitution of La^{3+} with Ag^+ in LaMnO_3 perovskite catalyst produced the oxygen vacancy as the active reaction site for the NO oxidation reaction with the concomitant transformation of Mn^{3+} to Mn^{4+} . The maximum solubility of Ag into the crystal structure of LaMnO_3 was achieved at around $x = 0.2$, where the highest amount of oxygen vacancies was formed. This information is also in good agreement to what have been obtained in this study, see Table 1.

3.7 Evaluation of soot-containing catalytic systems

DRIFT spectra recorded for soot-containing catalytic systems showed that the presence of soot modifies the nitrites and nitrates species distribution not only on catalyst surface but also on soot particle surface. Soot combustion experiments were carried over LaAgMnO_3 catalyst using different oxidizing environments (O_2 and NO/O_2) to evaluate the effect of NO and over LaMnO_3 under NO/O_2 atmosphere to assess the effect of silver incorporation. Fig. 9 shows the DRIFT spectra of soot combustion process carried out over LaAgMnO_3 under NO/O_2 atmosphere. Similar to what was observed from the catalytic experiments performed without soot (Fig. 6, Fig. 7 and Fig. 8), the first step for the catalytic activation corresponds to the elimination of adsorbed water from the catalyst surface during the first 200 °C. Almost simultaneously with water desorption, the signals associated to NO molecular adsorption or nitrosyl (1901 cm^{-1} and 1841 cm^{-1}) were seen. This result suggests that the adsorption/desorption events observed in Fig. 6 below 200 °C can be explained by the presence of this species. However, when temperature goes from 200 °C to 400 °C the signals associated to bridging bidentate nitrates (1610 cm^{-1}) and chelating bidentate nitrates (1587 cm^{-1}) becomes dominant along with signals associated to the molecular CO_2 (2280 cm^{-1} - 2400 cm^{-1}) and

bridging bidentate carbonates (1264 cm^{-1} - 1242 cm^{-1}) originated from soot oxidation. According to the CO_2 profile described in Fig. 5A, the soot oxidation over LaAgMnO_3 catalyst started at $180\text{ }^\circ\text{C}$, reached a maximum at $320\text{ }^\circ\text{C}$ and ended around $420\text{ }^\circ\text{C}$ being in good agreement with the DRIFTS results which also showed a similar behavior in the species distribution associated to molecular CO_2 and bridging bidentate carbonates. Note that the signal of bridging bidentate carbonate appears only when soot oxidation is taking place since before and after this process the signal is negative.

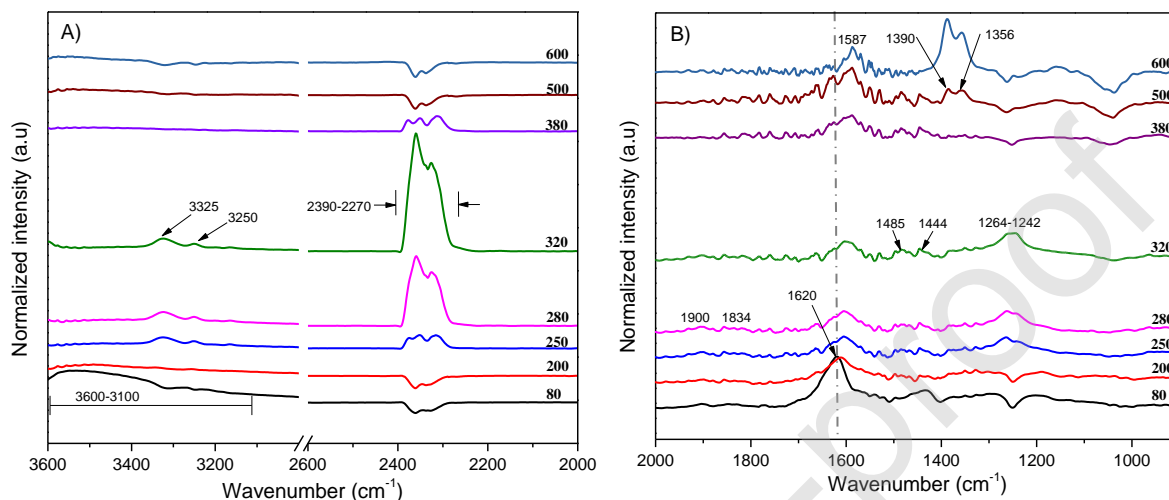


Fig. 9. DRIFT spectra of soot oxidation carried out over $\text{La}_{0.7}\text{Ag}_{0.3}\text{MnO}_3$ catalyst under NO/O_2 atmosphere (A) $2000\text{--}3600\text{ cm}^{-1}$ (B) $1000\text{--}2000\text{ cm}^{-1}$.

On the other hand, it is possible to see that above $400\text{ }^\circ\text{C}$ the signal associated to nitrites and bridging nitrates decreases almost completely while the one coming from chelating bidentate nitrates decreases slowly due to its high thermal stability [40,41,48,70]. Additionally, after soot oxidation completion a signal splitted in two bands (1390 cm^{-1} and 1356 cm^{-1}) was observed. As depicted in Table 2, they are attributed to free ionic nitrates (or Ag-nitrates species) and monodentate nitrates which are very stable at high temperature [40,48,70]. This result agrees to what has been observed in the catalytic test ($\text{LaAgMnO}_3 + \text{NO}/\text{O}_2$) without soot described in Fig. 8. The high thermal stability of free ionic nitrates and monodentate nitrates species even at $600\text{ }^\circ\text{C}$ is an indication of the good storage capacity of LaAgMnO_3 explaining why the NO concentration did not reach the reference value of 2000 ppm at the reactor outlet (see Fig. 5a). Previous studies performed on NO oxidation capacity over $\text{La}_{1-x}\text{Ag}_x\text{MnO}_3$ and NO -soot combustion over $\text{La}_{0.8}\text{Ce}_{0.2}\text{Mn}_{0.7}\text{Bi}_{0.3}\text{O}_3$ have proposed similar intermediate nitrates species having the following thermal stability decreasing order: chelating bidentate nitrates < bridging bidentate nitrates < monodentate nitrates < free ionic nitrates. They proposed that chelating bidentate nitrates and bridging bidentate nitrates can be easily decomposed below $400\text{ }^\circ\text{C}$ releasing NO_2 to the gaseous phase which is a stronger oxidant than molecular oxygen for soot oxidation [22, 40]. Although

monodentate nitrates and free ionic nitrates species can also contribute to soot oxidation in less extend, it must be considered NO_x storage species due to their thermal stability. In addition to this, we cannot rule out the participation of nitrites/hyponitrites or transient nitrates below 400 °C since although they were not seen around 1380 cm⁻¹ they could contribute to the NO₂ production that would explain the low ignition temperature for soot oxidation reported in Table 2.

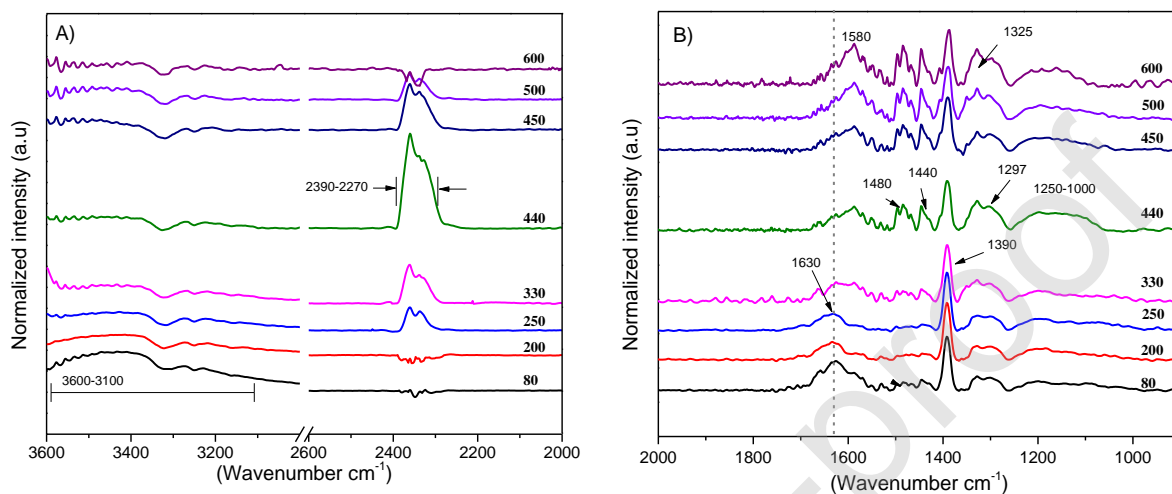


Fig. 10. DRIFT spectra of soot oxidation carried out over La_{0.7}Ag_{0.3}MnO₃ catalyst under O₂ atmosphere (A) 2000-3600 cm⁻¹ (B) 1000-2000 cm⁻¹.

In order to get some insights on the effect of NO on catalytic soot oxidation over LaAgMnO₃, Fig. 10 shows the DRIFT spectra of soot oxidation over LaAgMnO₃ catalyst with O₂ as a function of temperature. Since the catalytic system was not exposed to NO, all the IR signals are associated to different carbonates not only on the catalyst surface but also on soot surface. In general, after water desorption, signals coming from bridging bidentate carbonates (1630 cm⁻¹) and chelating bidentate carbonates (1580 cm⁻¹) were seen from temperature above 200 °C. In fact, it is observed that the signal associated to bridging bidentate carbonates was turned into chelating carbonates followed by a shift towards higher wavenumber as soot oxidation took place. Similarly, signals associated to free ionic carbonates on Ag-sites (1390 cm⁻¹) [60] and monodentate carbonates (1325-1297 cm⁻¹) were seen well above 200 °C, [22,61-65]. Those carbonates are very stable with temperature and can be easily formed on soot particles at the beginning of the reaction or stabilized on the surface of catalyst once soot oxidation took place. This behavior was not observed in LaAgMnO₃ under NO/O₂ atmosphere since it is believed that the presence of NO blocks the active sites by producing metal nitrates/nitrites species that decompose easily in the presence of soot and avoiding the readsorption of CO₂ on these sites. Other evidence that could tell us that NO adsorption is blocking the active sites for CO₂ coming from soot oxidation is the behavior of the signals associated to linear carbonates or monodentate carbonates (1484 cm⁻¹ and 1444 cm⁻¹). Note that these signals

increase as soot oxidation becomes important due to CO₂ re-adsorption a fact that was not observed in the test performed under NO/O₂ atmosphere. Finally, the signal associated to CO₂ originated from soot oxidation (2390 cm⁻¹-2270 cm⁻¹) coincides with the soot oxidation profile shown in Fig. 5B (see also table 2) where the maximum intensity of CO₂ evolution was achieved at 440 °C.

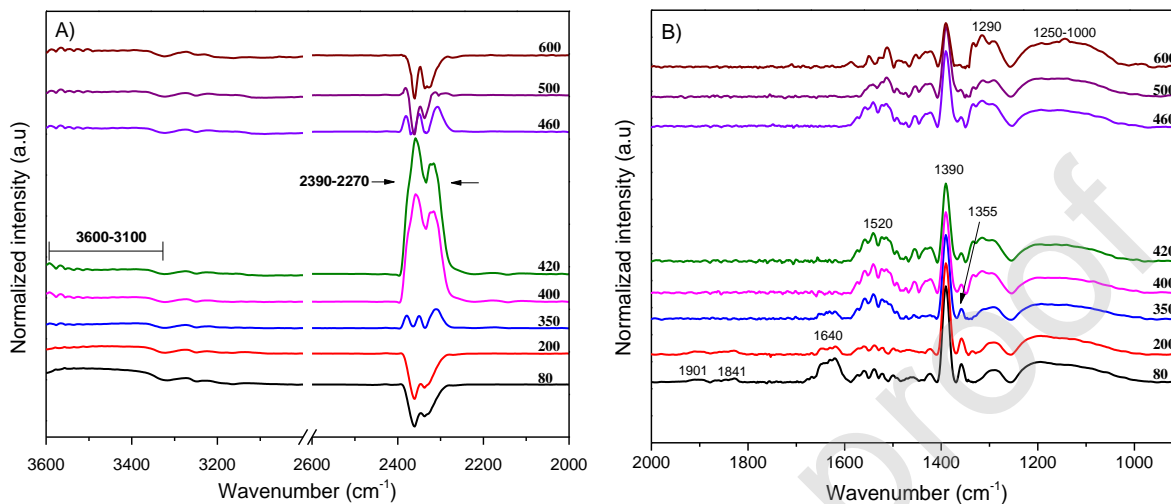


Fig. 11. DRIFT spectra of soot oxidation carried out over LaMnO₃ catalyst under NO_x/O₂ atmosphere (A) 2000-3600 cm⁻¹ (B) 1000-2000 cm⁻¹.

In order to further elucidate the contribution of silver incorporation on species distribution adsorbed on LaAgMnO₃ catalyst, a combustion experiment over LaMnO₃ under NO/O₂ atmosphere was carried out (see Fig. 11). In this Fig., the nitrogen and carbon species distribution was slightly different to what was observed over LaAgMnO₃ catalyst. In this case, the free ionic nitrate species formation took place at lower temperatures and its signal remained intense even within the temperature range for soot oxidation. This result suggests that in the absence of metallic silver, the NO can be preferentially adsorbed over the oxygen-occupied vacancies forming more stable nitrates with temperature than the ones formed on silver-containing perovskite catalyst surface. Taking this into account, the free ionic nitrates/nitrites species associated to Ag-sites observed in Fig. 9 are easily decomposed with temperature, releasing NO₂ almost immediately and explaining why it was not possible to see its adsorption in the IR below 400 °C. However, after silver nitrates decomposition on LaAgMnO₃ catalyst occurred, the contribution of more stable nitrates linked to oxygen-occupied vacancies becomes dominant as temperature increases. Another interesting feature observed in the spectra of LaMnO₃ catalyst is that the contribution of bridging and bidentate nitrates is scarce compared to the Ag-containing catalyst and most of the NO_x species are adsorbed as monodentate nitrates or nitro groups (1520 cm⁻¹). These species are the most involved in the soot oxidation process since their behavior with the signals associate to CO₂ evolution and monodentate

carbonate formation (1290 cm^{-1}) was pretty similar up to $500\text{ }^{\circ}\text{C}$. Although the IR signals of some carbonates species can be overlapped with those coming from nitrate species, the signal associated to gaseous CO_2 between $2270\text{-}2390\text{ cm}^{-1}$ coincides with the temperature range of soot oxidation with a maximum peak located at $420\text{ }^{\circ}\text{C}$. To recap, the soot oxidation process assisted by NO and followed by DRIFTS agrees with the TPD experiments shown in Fig. 5 with the following order in activity: $\text{LaAgMnO}_3 + \text{NO/O}_2 > \text{LaMnO}_3 + \text{NO/O}_2 > \text{LaAgMnO}_3 + \text{O}_2$.

4. Discussion

According to the previous results, at least four groups of nitrogenated species were demonstrated on the surface of the LaAgMnO_3 solid during the catalytic tests with and without soot under a NO/O_2 atmosphere including bridged bidentate nitrates and chelated bidentate nitrates, monodentate nitrites/nitrates and free ionic nitrite/nitrates species, besides those oxygenated and nitrogenated complexes that can also be formed on the surface of soot. The catalytic activity of this perovskite for the NO-assisted soot oxidation reaction depends on the stability of such nitrogenated species with temperature. The results described here suggest that bridged and chelated bidentate nitrates, as well as, some nitrites formed on oxygen-occupied vacancies and on silver sites decompose between $200\text{-}400\text{ }^{\circ}\text{C}$ releasing NO_2 , which rapidly reacts with soot particles to produce CO_2 and N_2 (Fig. 5A). On the other hand; the incorporation of Ag into the perovskite structure favored the segregation of La_2O_3 on the surface (see the XPS results) which in turn explains, at least in part, the improvement in the storage capacity of NO above $400\text{ }^{\circ}\text{C}$ through the formation of ionic nitrates and monodentate nitrates that could also involve Ag-sites.

To sum up, the reaction pathway postulated here agrees with what has been reported in literature [23], and suggests that there must exist a competition between molecular oxygen and gaseous NO for the active sites present on both surfaces (catalyst and soot particles) at low temperature ($25\text{ }^{\circ}\text{C}$ - $200\text{ }^{\circ}\text{C}$). This would explain the formation of the different oxygenated complexes $[\text{O}\cdot\text{O}]$, $\text{C}[\text{O}]$ and $\text{Ag}[\text{O}]$ that serve as anchoring points for the subsequent NO adsorption giving place to the formation of chelated and bridged bidentate nitrates $[\text{ONO}_2]$, as well as, silver nitrites $\text{Ag}[\text{NO}_2]$, [71]. These nitrogenated groups have been considered thermally unstable [40,41,48,70], so they would be the first to desorb as NO_2 in the range of temperatures in which soot oxidation take place ($200\text{ }^{\circ}\text{C}$ - $400\text{ }^{\circ}\text{C}$). In fact, the difference between LaAgMnO_3 and LaMnO_3 catalysts, it is that the additional NO_2 contribution coming from metallic silver sites speeded up the soot oxidation reaction.

$[\dots] + O_{2(g)} \rightarrow [O..O]$ $Cf + \frac{1}{2} O_{2(g)} \rightarrow C[O]$	$Ag_{(s)} + \frac{1}{2} O_{2(g)} \rightarrow Ag[O]$	Activation 25-200°C
$[O..O] + NO_{(g)} \rightarrow [ONO_2]$ $[ONO_2] + \frac{1}{2} O_{2(g)} \rightarrow NO_{2(g)} + [O..O]$	$Ag[O] + NO_{(g)} \rightarrow Ag[NO_2]$ $Ag[NO_2] + \frac{1}{2} O_2 \rightarrow Ag[O] + NO_{2(g)}$	NO ₂ release and soot oxidation 200-400 °C
$Cf + NO_{2(g)} \rightarrow C[NO_2]$ $C[O] + NO_{(g)} \rightarrow C[ONO]$ $C[NO_2] + C[ONO] \rightarrow CO_{2(g)} + N_{2(g)}$		NO ₂ release and soot oxidation 200-400 °C
$[O..O] + NO_{(g)} \rightarrow [ONO_2]^*$	$Ag[O] + \frac{1}{2} O_{2(g)} + NO_{(g)} \rightarrow AgNO_{3(s)}$	NO storage 400-600 °C

[..] = oxygen vacancy sites on LaAgMnO₃ perovskite, [O..O] = oxygen on oxygen vacancy, Cf = soot, Ag_(s) = metallic silver site, [ONO₂] = chelating and bridging nitrates, Ag[NO₂] = silver nitrite also hyponitrites, C[NO₂] = organic nitro, C[ONO] = organic nitrite, [ONO₂]* = linear or monodentate nitrate, free ionic nitrate, AgNO_{3(s)} = Silver nitrate.

Although the previous description refers to what happens on the surface of the catalyst, we cannot rule out the formation of nitro group species, C[NO₂], on the active surface of soot through the adsorption of NO on previously formed oxygenated carbon complexes C[O]. It is worth mentioning that the infrared signals for the nitro groups and oxygenated complexes formed in the soot overlap with the signals of the complexes formed on the catalyst, so in the IR spectra of the catalyst systems containing soot there is a contribution from both groups. Due to the simultaneous removal of soot and NO, it is feasible to think that in the reactive interface, the NO₂ transfer is given from the catalyst to soot particles increasing the amount of organic nitro complexes (C-NO₂) that when they are close enough can be reorganized to form CO₂ and N₂ as the main products of the TPD. Once the soot oxidation ends, the adsorption of NO continues through a storage process on the surface of the catalyst mediated by the formation of silver nitrate Ag[NO₃], [22] and/or monodentate nitrates

[ONO₂]* resulting from the transformation of bidentate bridge-type nitrates when the temperature is higher than 400 ° C [40,41,48,70]..

In line with the reaction pathway presented above, both oxygen vacancies and metallic silver sites are active for NO oxidation and adsorption over LaAgMnO₃ catalyst. For a better understanding of the role of both active sites some research works that have evaluated surface-doped and –dispersed silver in perovskite systems (e.g., Ag/LaMnO₃ vs LaAgMnO₃ vs LaMnO₃) for the oxidation of different contaminants were referenced [72,73]. According to these authors, the silver segregation on catalytic surface can enhance the spill-over phenomena facilitating the active oxygen species formation and transfer compared to the bare catalyst, while the incorporation of silver into the perovskite structure led to an increase in the oxygen vacancies formation. Considering the catalytic activity of both systems (dispersed and incorporated silver), the one with surface-dispersed metal showed the best catalytic activity toward oxidation of the contaminants as it was evidenced by Albaladejo-Fuentes et al. [3] on the NO oxidation experiments toward NO₂. They also indicated that the presence of oxygen vacancies on the catalyst surface increased the NO_x storage capacity, i.e. NO-adsorption was favored. Although surface-dispersed metals seem to be more active than the oxygen vacancies for NO oxidation, Yoon et al. [22] suggested in an implicit way that a balance between dispersed and doped silver on catalyst surface should be established to maximize its catalytic activity. They found that the rate constant for NO oxidation reached its maximum when the solubility of Ag into the crystal structure of LaMnO₃ was achieved at around $x = 0.2$, (highest amount of oxygen vacancies) whereas the contrary effect on the rate constant was found when the molar fraction of silver increased from 0.2-0.8 due to an increase of both metallic silver segregation and silver particle size causing a reduction on surface area. In our work, we have decided to evaluate the combined effect of both active sites since they contribute in some extent to the NO oxidation that will also impact the soot oxidation.

5. Conclusions

The incorporation of silver into the perovskite structure favored the simultaneous removal of soot and NO_x by displacing the oxidation peak at low temperatures with an activation energy of 55 kJ/mol compared to the non-catalytic one of 81 kJ/mol. Likewise, the presence of NO in the catalytic system favored the formation of different types of nitrates helping in the activation of both catalyst and soot surfaces, and accelerated the oxidation reaction of carbonaceous material. According to the results, at temperatures below 200 °C the activation of the catalyst and soot surfaces occurs through a competitive process between molecular oxygen and gaseous NO_x for the

active sites. In fact, the weakly adsorbed NO (or nitrosyl) on catalyst surface has a maximum desorption peak at 180 °C that coincided with the ignition temperature of soot oxidation and with the appearance of bridging, chelating and free ionic nitrite/nitrate species on silver sites that later decompose as NO₂ in the temperature range between 200 °C and 400 °C. Also, a good NO_x storage capacity on the silver-containing system was evidenced since above 400 °C, only the monodentate nitrates and possibly Ag-Nitrates increased in proportion, and explaining why the NO profile in the TPD experiments did not reach the reference value of 2000 ppm.

The reaction mechanism is similar to those proposed in references a and b, after the heat treatment, the molecular oxygen is dissociatively adsorbed on catalyst vacancies and soot active sites forming oxygen complexes, then the NO is adsorbed on such active sites forming nitrite/nitrate species on catalyst surface and nitro organic complexes on soot surface. It is known that inorganic nitrates are less thermally stable and decompose rapidly as NO₂ (a stronger oxidant than O₂) which can be transferred to the carbonaceous material through soot-catalyst interface increasing the amount of nitro complexes that when they are close enough can be reorganized to form CO₂ and N₂ as the main products of the redox reaction.

In the silver-free catalyst, although the nitrogenous complexes were similar, the absence of silver makes the formation of monodentate nitrates (over oxygen in vacancies) more important even at low temperatures. It is likely that the soot oxidation in this catalyst will also be mediated through NO₂, but in less proportion than that observed in the catalyst-containing silver. It is also important to mention that in the absence of silver, the LaMnO₃ catalyst lost its storage capacity since the incorporation of silver favors the La segregation as La₂O₃ which has a high capacity to retain NO at high temperatures.

Declarations of interest

none

Acknowledgements

The authors want to thank the University of Antioquia for the financial support received through the CODI project No 2015-7828. L.U. thanks the Colombian Administrative Department of Science, Technology and Innovation (COLCIENCIAS), for the Ph.D. Scholarship granted.

References

- [1] İ.A. Reşitoğlu, K. Altinişik, Keskin.A, *Clean Technol. Environ. Policy* 17 (2015) 15–27.
- [2] F.J. Kelly, J.C. Fussell, *Environ. Geochem. Health* 31 (2015) 631–649.
- [3] N.M. Liu, J. Grigg, *BMJ Paediatr. Open* 2 (2018).
- [4] <https://www.epa.gov/transportation-air-pollution-and-climate-change/smog-soot-and-local-air-pollution>, accessed May 13, 2019
- [5] K. Okude, K. Mori, S. Shiino, T. Moriya, *SAE Tech. Pap.* (2004).
- [6] C.D. Nam, *Eur. J. Eng. Res. Sci.* 3 (2018) 32–36.
- [7] C. Xu, H. Cho, *Int. J. Eng. Technol.* 7 (2018) 1519–1526.
- [8] V. Bermúdez, J.M. Luján, H. Climent, L. Soto, D. Campos, *SAE Int. J. Engines* 11(03-11–0 (2018).
- [9] M. Piumetti, S. Bensaid, D. Fino, N. Russo, *Catal. Struct. React.* 1 (2015) 155–173.
- [10] J. Schobing, V. Tschamber, J.F. Brillhac, A. Auclair, Y. Hohl, *Comptes Rendus Chim.* 21 (2018) 221–231.
- [11] L. Lietti, L. Castoldi, *R. Soc. Chem.* 33 (2018).
- [12] C. Davies, K. Thompson, A. Cooper, S. Golunski, S.H. Taylor, M.B. Macias, A. Tsolakis, *Appl. Catal. B Environ.* 239 (2018) 10–15.
- [13] G.C. Dhal, S. Dey, D. Mohan, R. Prasad, *Catal. Rev.* (2018) 1–60.
- [14] A. Setiabudi, M. Makkee, J.A. Moulijn, *Appl. Catal. B Environ.* 50 (2004) 185–194.
- [15] F. Bin, C. Song, G. Lv, X. Li, J. Song, S. Wu, *Proc. Combust. Inst.* 35 (2015) 2241–2248.
- [16] N. Guillén-Hurtado, A. García-García, A. Bueno-López, *J. Catal.* 299 (2013) 181–187.
- [17] Z. Wang, X. Yan, X. Bi, L. Wang, Z. Zhang, Z. Jiang, Q. Wang, *Mater. Res. Bull.* 51 (2014) 119–127.
- [18] I. Atribak, B. Azambre, A. Bueno-López, A. García-García, *Appl. Catal. B Environ.* 92 (2009) 126–237.
- [19] W.F. Shangguan, Y. Teraoka, S. Kagawa, *Appl. Catal. B Environ.* 12 (1997) 237–247.
- [20] H. Zhu, J. Xu, Y. Yichuan, Z. Wang, Y. Gao, W. Liu, H. Yin, *J. Colloid Interface Sci.* 508 (2017) 1–13.
- [21] L. Ai, Z. Wang, C. Cui, W. Liu, L. Wang, *Materials (Basel)*. 11 (2018).
- [22] D. Yoon, E. Lim, Y.J. Kim, J.H. Kim, T. Ryu, S. Lee, B.K. Cho, S. Yoo, *J. Catal.* 319 (2014) 182–193.
- [23] L. Urán, J. Gallego, W. Li, A. Santamaría, *Appl. Catal. A Gen.* 569 (2019) 157–169.
- [24] R. Ran, D. Weng, X. Wu, J. Fan, L. Qing, *Catal. Today* 126 (2007) 394–399.

- [25] M.N. Iliev, M. V Abrashev, V.N. Popov, V.G. Hadjiev, *Phys. Rev. B* 67 (2003) 212–301.
- [26] J.A. Onrubia, B. Pereda-Ayo, U. De-La-Torre, J.R. González-Velasco, *Appl. Catal. B Environ.* 213 (2017) 198–210.
- [27] T. Andana, M. Piumetti, S. Bensaïd, L. Veyre, C. Thieuleux, N. Russo, R. Pirone, *Appl. Catal. B Environ.* 216 (2017) 41–58.
- [28] R. Dinamarca, X. Garcia, R. Jimenez, J.L.G. Fierro, G. Pecchi, *Mater. Res. Bull.* 81 (2016) 134–141.
- [29] S. Ponce, M.A. Pena, J.L.G. Fierro, *Appl. Catal. B Environ.* 24 (2000) 193–205.
- [30] B. Kucharczyk, W. Tylus, *Appl. Catal. A Gen.* 335 (2008) 28–36.
- [31] N. Zouaoui, M. Issa, D. Kehrlı, M. Jeguirim, *Catal. Today* 189 (2012) 65–69.
- [32] J. Giménez-Mañogil, A. García-García, *Fuel Process. Technol.* 129 (2015) 227–235.
- [33] A.M. Hernández-Giménez, L.P. dos Santos Xavier, A. Bueno-López, *Appl. Catal. A Gen.* 462 (2013) 100–106.
- [34] I.S. Pieta, M. García-Diéguez, C. Herrera, M.A. Larrubia, L.J. Alemany, *J. Catal.* 270 (2010) 256–267.
- [35] B. Klingenberg, M.A. Vannice, *Chem. Mater.* 8 (1996) 2755–2768.
- [36] T. Yousefi, A.N. Golikand, M.H. Mashhadizadeh, M. Aghazadeh, *Curr. Appl. Phys.* 12 (2012) 193–198.
- [37] N. Tang, Y. Liu, H. Wang, Z. Wu, *J. Phys. Chem. C* 115 (2011) 8214–8220.
- [38] Y. Liu, H. Dai, J. Deng, L. Zhang, Z. Zhao, X. Li, Y. Wang, S. Xie, H. Yang, G. Guo, *Inorg. Chem.* 52 (2013) 8665–8676.
- [39] C.A. da Silva, P.E. V de Miranda, *Int. J. Hydrogen Energy* 40 (2015) 10002–10015.
- [40] F. Bin, G.L. Song, J. Song, K. Wang, X. Li, *Proc. Combust. Inst.* 34 (2013) 2303–2311.
- [41] J. Qian, X. Hou, F. Wang, Q. Hu, H. Yuan, L. Teng, B. Li, *J. Phys. Chem. C* 122 (2018) 2097–2106.
- [42] K. Liu, F. Liu, L. Xie, W. Shan, H. He, *Catal. Sci. Technol.* 5 (2015) 2290–2299.
- [43] A. Bueno-López, D. Lozano-Castelló, A.J. McCue, J.A. Anderson, *Appl. Catal. B Environ.* 198 (2016) 266–275.
- [44] X. Yao, L. Li, W. Zou, S. Yu, J. An, H. Li, F. Yang, L. Dong, *Chinese J. Catal.* 37 (2016) 1369–1380.
- [45] S. Liu, X. Wu, D. Weng, M. Li, R. Ran, *ACS Catal.* 5 (2015) 909–919.
- [46] M. Kantcheva, M. Milanova, S. Mametsheripov, *Catal. Today* 191 (2012) 12–19.
- [47] J.J. Yu, Z. Jiang, L. Zhu, Z.P. Hao, Z.P. Xu, *J. Phys. Chem. B* 110 (2006) 4291–4300.
- [48] C. Sedlmair, K. Seshan, A. Jentys, J.A. Lercher, *J. Catal.* 214 (2003) 308–316.

- [49] F.E. López-Suárez, M.J. Illán-Gómez, A. Bueno-López, J.A. Anderson, *Appl. Catal. B Environ.* 104 (2011) 261–267.
- [50] X. Zeng, X. Huo, T. Zhu, X. Hong, Y. Sun, *Molecules* 21 (2016) 1491.
- [51] W.A.N.G. Lei, R.A.N. Rui, W.U. Xiaodong, L.I. Min, W.E.N.G. Duan, *J. Rare Earths* 31 (2013) 1074–1080.
- [52] Z. Zhang, Y. Zhang, Q. Su, Z. Wang, Q. Li, X. Gao, *Environ. Sci. Technol.* 44 (2010) 8254–8258.
- [53] F. Prinetto, G. Ghiotti, I. Nova, L. Lietti, E. Tronconi, P. Forzatti, *J. Phys. Chem. B* 105 (2001) 12732–12745.
- [54] P. Li, L. Feng, F. Yuan, D. Wang, Y. Dong, N. Xiaoyu, Y. Zhu, *Catalysts* 6 (2016) 124.
- [55] S. Bernal, J. Botana, R. García, J. Rodríguez-Izquierdo, *Thermochim. Acta* 66 (1983) 139–145.
- [56] J. Szanyi, J.H. Kwak, *Chem. Commun.* 50 (2014) 14998–15001.
- [57] M. Mihaylov, E. Ivanova, H. Aleksandrov, P. Petkov, G. Vayssilov, K. Hadjiivanov, *Mol. Catal.* (2018).
- [58] B. Azambre, S. Collura, J. M. Trichard, J. V. Weber, *Appl. Surf. Sci.* 253 (2006) 2296–2303.
- [59] H. Muckenhuber, H. Grothe, *Carbon N. Y.* 45 (2007) 321–329.
- [60] M. Haneda, Y. Kintaichi, M. Inaba, H. Hamada, *Catal. Today* 42 (1998) 127–135.
- [61] O. Seiferth, K. Wolter, B. Dillmann, G. Klivenyi, H.-J. Freund, D. Scarano, A. Zecchina, *Surf. Sci.* 421 (1999) 176–190.
- [62] E.-M. Köck, M. Kogler, T. Bielz, B. Klötzer, S. Penner, *J. Phys. Chem. C* 117 (2013) 17666–17673.
- [63] D. Cornu, H. Guesmi, J.-M. Krafft, H. Lauron-Pernot, *J. Phys. Chem. C* 116 (2012) 6645–6654.
- [64] J.C.S. Wu, C.-W. Huang, *Front. Chem. Eng. China* 4 (2010) 120–126.
- [65] H. Li, X. Jiao, L. Li, N. Zhao, F. Xiao, W. Wei, Y. Sun, B. Zhang, *Catal. Sci. Technol.* 5 (2015) 989–1005.
- [66] B.H. Solis, Y. Cui, X. Weng, J. Seifert, S. Schauerermann, J. Sauer, S. Shaikhutdinov, H.-J. Freund, *Phys. Chem. Chem. Phys.* 19 (2017) 4231–4242.
- [67] S.K. Hussain, G. Nagaraju, E. Pavitra, G. Seeta Rama Raju, J.S. Yu, *CrystEngComm* 17 (2015) 9431–9442.
- [68] J. Ding, Y. Wu, W. Sun, Y. Li, *J. Rare Earths* 24 (2006) 440–442.
- [69] B. Jaleh, P. Fakhri, *Spectrosc. Polym. Nanocomposites William An* (2016) 112–129.
- [70] M. Kantcheva, *Appl. Catal. B Environ.* 42 (2003) 89–109.

- [71] M. Anbar, M. Halmann, S. Pinchas, *J. Chem. Soc.* (1960) 1242–1245.
- [72] S. Megarajan, S. Rayalu, M. Nishibori, Y. Teraoka, N. Labhsetwar, *ACS Catal.* 5 (2014) 301–309.
- [73] O. Buchneva, I. Rossetti, C. Biffi, M. Allieta, A. Kryukov, N. Lebedeva, *Appl. Catal. A Gen.* 370 (2009) 24–33.
- [74] V. Albaladejo-Fuentes, F.E. López-Suárez, M.S. Sánchez-Adsuar, M.J. Illán-Gómez, *Appl. Catal. A Gen.* 519 (2016) 7–15.

Table 1. Surface atomic ratios obtained from the XPS spectra of $\text{La}_{0.7}\text{Ag}_{0.3}\text{MnO}_3$ and LaMnO_3 perovskite-like catalysts

Sample	Ag/Mn ^a	Ag _{perov}	Ag ⁰ /Ag _s ^b	Mn ³⁺	Mn ⁴⁺	Mn ⁴⁺ /Mn ³⁺	O _β	O _α
LaMnO ₃	0.00	0.00	0.00	0.41	0.35	0.85	0.55	0.24
LaAgMnO ₃	0.56	0.81	0.30	0.31	0.40	1.28	0.65	0.30

^a Nominal stoichiometric ratios for LaMnO₃ (La/Mn = 1) and LaAgMnO₃ (La/Mn = 0.7 and Ag/Mn = 0.3)

^b Ag_s is the total silver non-incorporated into perovskite-like lattice, i.e. Ag₂O+Ag⁰.

Table 2. Reaction parameters associated to soot oxidation under different atmospheres

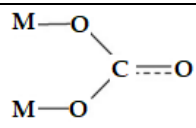
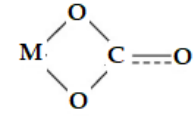
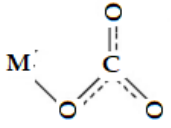
System	T _{window}	T _{ig} (°C)	T _{peak} (°C)	S _{CO2} (%)	E _a ^a (kJ/mol)	NO _{conv} (%)
LaAgMnO ₃ -soot NO/O ₂	200-400	124	327	100	54.11	60
LaAgMnO ₃ -soot O ₂	200-530	133	442	100	73.3	N/A
LaMnO ₃ -soot NO/O ₂	200-470	250	375	92	65.2	25
Non-catalytic NO/O ₂	150-650	277	645	40	87.8	1

^a E_a for soot oxidation applying the Ozawa methodology (see Fig.S5).

Table 3. Assignment of IR bands to surface species during the simultaneous NO_x and soot removal

NO _x complexes on catalyst and soot surface				
Signal assignment	Structure	Vibration	Wavenumber	References
Adsorbed water		OH _(as, s) OH _(bending)	3600-2800 1625	[19,22, 33-39]
Nytrosil	$M-N\equiv O^+$	N≡O M-N	1903 1841	[19,37,40,41]
Bridged nitrate		N=O NO ₂ (as and s)	1625 1300-1260	[17,19,33 40-50]
Chelated nitrate		N=O NO ₂ (as)	1587 1300-1260	[19,22,34,35,37, 40,42-45,47-49,51]
Monodentate nitrate (Linear nitrates)		N=O NO ₂ (as) NO ₂ (s)	1530 1484-1444 1350-1260	[16, 19,20,22,33-35,40,42,43,45,47-51]
Monodentate nitrite	$M-O-N=O$	N=O NO ₂ (as) NO ₂ (s)	1520-1460 1330-1370 ^(a) 1264-1242 ^(a)	[17,22,34,44-49,52,53]
Nitro		NO ₂ (as) NO ₂ (s)	1530-1460 1370-1330	[43,44,49,50]
Hyponitrite		N-N	1380-1330	[25,41,48,54-57]
Free ionic nitrate	$M^+ \left[\begin{array}{c} O \\ \\ N \\ / \backslash \\ O \quad O \end{array} \right]^-$	NO ₂ (as)	1380	[22,33,34,35,39, 41,44,52]
Free ionic nitrite	$M^+ \left[\begin{array}{c} O \\ \\ N \\ \backslash \\ O \quad O \end{array} \right]^-$	NO ₂ (s) NO ₂ (as)	1330 1250	[34,53]
Organic nitro group	C-NO ₂	N=O NO ₂ (s)	1625 1380	[41,45,58-60]
Organic nitrites	C-ONO	N=O	1625	[58-60]

a = overlapped with bridging and chelating nitrites

CO _x complexes on both catalyst surface and soot surfaces				
Gaseous CO ₂	O-C=O	C=O _(as)	2390-2270	[34,40,41,61-66]
Bridged carbonate		C=O	1625	[52,61-63]
		CO ₂ _(as)	1260	
Chelated carbonate		C=O	1530	[22,39,44,48,50,61-66]
		CO ₂ _(as)	1330-1370	
Ionic carbonate	CO ₃ ²⁻		1353	[52,61-66]
Monodentate carbonate		C=O	1530-1460	[22,35,43,44,61-65]
		CO ₂	1330-1370	
Carbonyl	R-C=O	C=O	1625	[45,59,65]